BULLETIN OF THE POLISH ACADEMY OF SCIENCES
TECHNICAL SCIENCES, Vol. 62, No. 1, 2014
DOI: 10.2478/bpasts-2014-0017

Experimental and numerical study of influence of incidence angle of shock wave created by explosive charge on the steel plate

W. BARNAT*

Department of Mechanics and Applied Computer Science, Military University of Technology,
2 Gen. Sylwestra Kaliskiego St., 00-908 Warsaw, Poland

Abstract. This paper presents experimental and numerical studies on influence of an incidence angle of the shock wave on a steel plate. The problem of interaction between the wave front and a barrier is important from the point of view of protection the crew of armored vehicles. One way of remedying the harmful effects of impacts of the shock wave is the reflection wave of the barrier set at an angle to the face of the wave. The article presents the numerical and experimental approach to the subject. The numerical part presents four models in which the plate was set at angles 0°, 15°, 30°, 45°. In each case, the plate was loaded by a wave formed after the explosion 2 kg of TNT. In the experimental part the results are presented from an experiment in which the wave was formed from 2 kg TNT detonation at a distance of 0.4 m in parallel to the steel plate.

Key words: blast, blast protection, structural response, FEM.

1. Introduction

Numerical and experimental studies of structures loaded by a shock wave (pressure impulse) are burdened with many experimental, numerical and analytical errors. A phenomenon of impact of a pressure impulse into a flat barrier has been described quite extensively. In the case of an impact of a shock wave into a plate positioned at a certain angle, there are known only a few analytical works [1, 2].

The blast impact into flat plates was widely reported with satisfactory results in numerical and experimental approaches [3–5].

In a place where the front of the blast wave is not perpendicular to a barrier, small number studies have been published in open literature [6–8].

In the case of a numerical analysis, there are a few approaches to a dynamic phenomenon. The first approach is related to vibration of the structure [9, 10]. Modern science considers the approach to a numerical analysis of both implicit and explicit type. These approaches are associated with the duration of an impulse and with the frequency of vibrations of an object [11, 12]. When the impulse duration is shorter than the period of natural vibrations of the object, the problem is solved by an explicit method.

The main problem in a numerical analysis is an appropriate choice of material properties and load parameters. In the case where load parameters are considered, analytical methods are often used [13]. These methods are based on many complex formulas and experiments [14, 15].Additionally, analytical methods are consistent when a pressure wave hit into a flat barrier usually oriented perpendicularly in front of the charge. It is advisable to verify numerical investigations with experimental studies [16]. To a large extent, numerical methods are burdened with a considerable error in the case of an impact into a susceptible barrier oriented at a certain angle or with a very complex shape. The purpose of the paper is to present the results of numerical research performed by the author in light of other studies on the effects of a placement angle of the plate on the dynamic response of the plate. Methods for estimating the shock wave are widely presented in world literature. Therefore, in this article, the author omits a description of the above mentioned phenomenon. An extensive theoretical description of the phenomenon of the pressure impulse interaction onto a barrier is caused by an intention to clarify the mechanisms acting during a shock wave impact on all sorts of barriers. The article discusses wider the phenomena of the impulse pressure reflection.

1.1. Basic characteristics of the shock wave coming from the explosion.

The impact of explosion on the structure depends on the characteristics of the pressure impulse of a shock wave that is generated by the detonation of an explosive [17]. Figure 1 shows the ideal course of pressure in time for a place located at a certain distance from the center of the explosion.

It is interesting that in some distance from the epicenter of the explosion, there occurs a sudden increase in pressure of value $p+$ – maximum pressure value at the wave front.

This value increases p_0 – pressure value for an undisturbed medium. A supplementary parameter characterizing the positive phase of pressure is its duration time τ^+.

In addition, a passage of the shock wave is followed by the negative phase of pressure (vacuum), p – also called a vacuum. It is described by the time τ^-. Complementary parameters of the pressure impulse is t_a – time of arrival of the shock wave front.

*e-mail: wbarnat@o2.pl

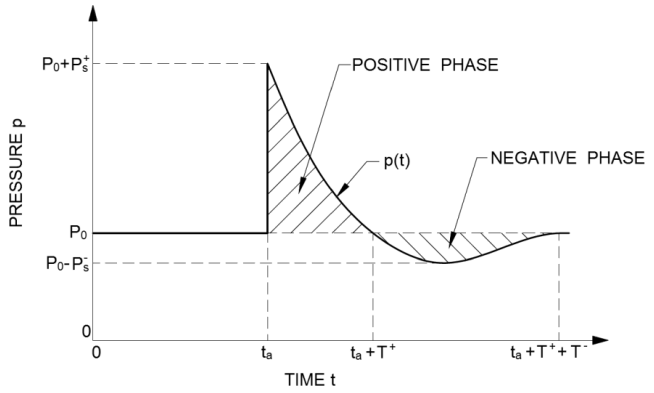

Fig. 1. Course of ideal pressure during detonation after Ref. 17

In the early phase of the shock wave formation, a wave moves together with the products of explosion (detonation) at a very high speed. As the wave front propagates, the pressure and the velocity decrease as a result of spreading of the surface wave over greater and greater volume of the medium in which the wave propagates. For a sufficiently long distance from the center of explosion, the interaction between the wave and detonation products ceases completely [13]. Depending on the parameters of a wave, the speed of the pressure impulse can be both the lower and higher value than the speed of a sound.

1.2. The impact of the shock wave on a barrier – a rebound effect. So far, many articles about estimation of the pressure impulse have been published. These studies were mainly based on the assumption that explosion was considered mostly as a point phenomenon. The publications rarely relate to the issues of reflection, particularly multiple reflection.

The following types of reflections can be distinguished:

- Normal reflection;
- Reflection at an angle;
- Mach reflection.

Normal reflection. One of the simplest cases of reflection from a rigid barrier is reflection at an angle of 90 degrees. Such a case is shown in Fig. 2. The pressure on the surface of the wall is normally determined as a "reflection" overpressure, and marked with the symbol P_r. For very weak pressure waves, $P_s \ll P_0$, the increase of the pressure impulse is twice the increase, $P_r = 2P_s$. For higher values of pressure, the value of reflected pressure is significantly greater. The upper limit is often reported in the literature $P_0 = P_r * 8P_s$. This limit applies to the air treated as an ideal gas, even at high pressures.

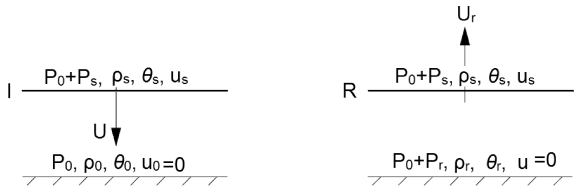

Fig. 2. Diagram of regular perpendicular reflection from the rigid barrier after Ref. 17

Another phenomenon of reflection is so-called oblique reflection from a rigid flat barrier.

Oblique reflection. Another case of the wave reflection is an oblique reflection from the barrier. This case is shown and presented in Fig. 3. The shock wave moves in the undisturbed medium (Region 1) at the speed U. The wave front and the barrier makes an angle α_I. Behind the front of the shock wave (Region 2) there occur prevailing condition areas after passing a plane wave through the undisturbed medium. After making a contact with the barrier, a flow behind the wave turned, because the normal component to the wall must be zero and the wave is reflected from the wall at an angle α_R, not always equal to α_I. Symbols in Region 3 correspond to the reflected wave.

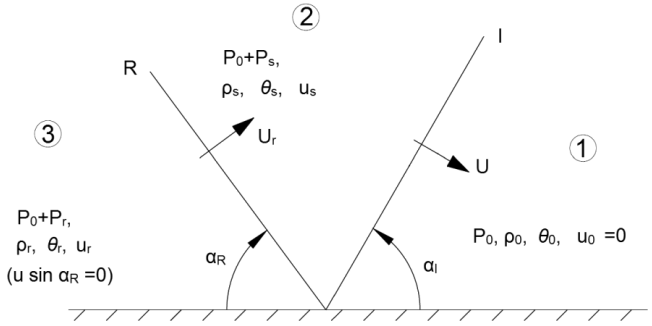

Fig. 3. Regular oblique reflection from a rigid wall after Ref. 17

Such a type of reflection can lead to the amplification of the pressure impulse [2, 13]. The shock wave is reflected while falling on the barrier. During the reflection, there may occur amplification of a pressure impulse of reflected wave P_r, which can be a multiple of pressure of the incident wave P_s [18]. The relationship of the amplification factor of C_r pressure values depending on an angle α_1 is shown in Fig. 4.

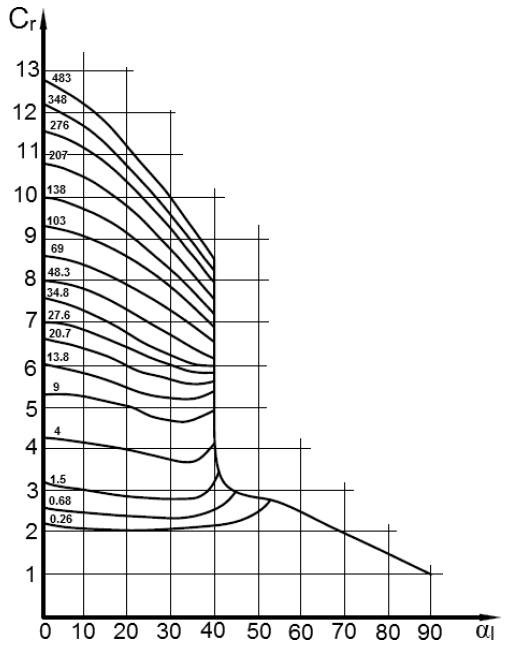

Fig. 4. Relationship of pressure impulse amplification (C_r ratio) depending on an angle of incidence α_1 after Ref. 18

The pressure of the reflected wave P_r, as resulted from Fig. 4, reaches the maximum value for an angle of incidence of 0°. The angle equals to 40°. For such an angle, the pressure of the reflected impulse decreases.

For the analytical determination of a pressure change of a shock wave in contact with a barrier, a number of simplifications and assumptions is taken:

1. A barrier is not deformable and static.
2. The barrier is positioned perpendicularly to the direction of wave propagation.
3. An explosion occurs immediately in a highly rarefied medium (in the air, not liquid).
4. Dimensions of the barrier are endless and they prevent the barrier from the wave flow.
5. The pressure transmitted by a wave is a sum of two components: static and dynamic.

At the moment of contact of a shock wave with the barrier, a new wave (reflected wave) spreading throughout in the opposite direction of the incident wave (free wave) is originated. The reflected wave spreads in the already disturbed medium (directions of movement of gas particles are in accordance with the direction of the incident wave), hence the pressure on the forehead of the reflected wave is greater than that of the incident wave. A formula for the maximum pressure of the reflected wave is shown below [19]:

$$\Delta p_2 = 2\Delta p_1 + \frac{6\Delta p_1^2}{\Delta p_1 + 7p_0}, \tag{1}$$

where Δp_1 – overpressure of free wave, Δp_2 – overpressure of reflected wave, p_0 – air pressure.

Equation (1) shows that when the pressure wave is $\Delta p_1 \gg p_0$ is:

$$\frac{p_2}{p_1} = 8 \tag{2}$$

on the forehead of the reflected pressure even it is eight times stronger. In the case of very weak waves, when $\Delta p_1 < p_0$ from 1

$$\frac{p_2}{p_1} = 2 \tag{3}$$

that is, at the reflection of waves of small intensities, over pressure on the forehead of the reflected wave is doubled, which corresponds to the phenomenon of the acoustic wave reflection.

1.3. Analytical method for determining a pressure impulse acting on the barrier. The determination of the total load with an impulse pressure derived from explosion of an element of the construction requires the determination of the total impulse generated by the blast of the load. The task is reduced to the integration of a unit load impulse on the surface affected by the explosion load [1]:

$$J = \int_F^{idF}, \tag{4}$$

where i – unit impulse, F – area of barrier.

Computational scheme for a spherical load located over the circular plate is presented in Fig. 5. Based on the literature, it was found that a total impulse generated by explosion, in this case [1], is equal to:

$$J = \pi \cdot A_0 \cdot C \cdot \sin^2 \alpha_0, \tag{5}$$

where J – is the total impulse of force expressed in newton-seconds, A_0 – is a constant characterizing the explosive (for TNT it is 387–410 m/s), C – is the mass of the load in kilograms.

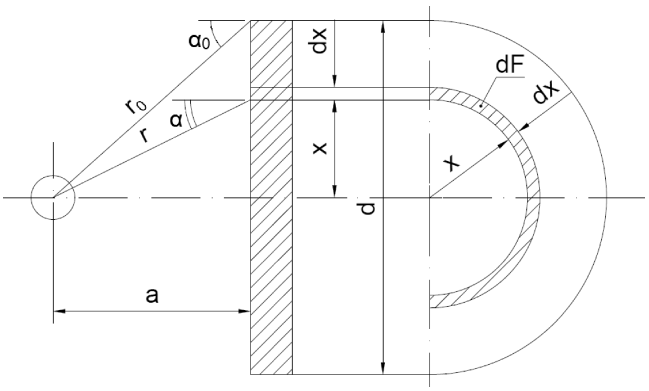

Fig. 5. Scheme for determining impulse acting on the circular disc after Ref. 1

Other cases are considered in a similar manner. There is a formula taking into account the maximum cross-section of the barrier as well as its shape. The form of this formula is as follows:

$$J = k_f \cdot S \cdot i_0, \tag{6}$$

where S – is the maximum cross-sectional area to the gas flow direction, k_f – is the ratio of transverse shape of the barrier $k_f = 1$ – for a plate arranged perpendicularly to the flow, $k_f = \frac{1}{2}$ – for a plate located diagonally across the flow, and for the sphere, $k_f = \frac{2}{3}$ – for a barrier in the form of a cylinder, i_0 – is a unit impulse of the flow.

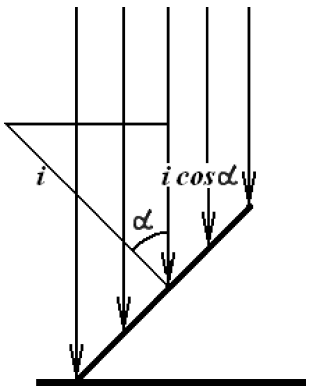

Fig. 6. Scheme of unit impulse impact on a barrier in the form of a plate set obliquely

The preliminary analysis of the expression (6) shows that the barriers in the form of spheres and plates (beams in the

shape of the letter "V") receive twice as less load than a plate located flatwise (of course, for the same conditions: the mass of explosive and the distance of the maximum cross section). This phenomenon is used in the design of structures exposed to mines and improvised explosive devices (IEDs) effects.

2. Objects of research

During the dynamic tests, the validation experiment and four numerical tests were performed. The comparison of the variants of tested objects are presented in Table 1.

Table 1
Comparison of analyzed cases

Test	Load	Load distance from the base plate	Inclination angle of plate	Type of research
1	2 kg	0.4 m	0°	The numerical / experimental
2			15°	The numerical
3			30°	The numerical
4			45°	The numerical

All experimental studies were carried out during the implementation of the research work managed by the author himself [20]. The test ground consisted of a frame and a steel plate with thickness of 5 mm. The elements of the test ground were made of steel S235JR2 (according to the European standard EN 10025:1990).

An exemplary test result is shown in Fig. 7. In addition, a series of material research on the Hopkinson rod was conducted to determine dynamic properties of the material. Tests for steel S235JR2 were carried out at the Department of Mechanics and Applied Computer Studies, MUT.

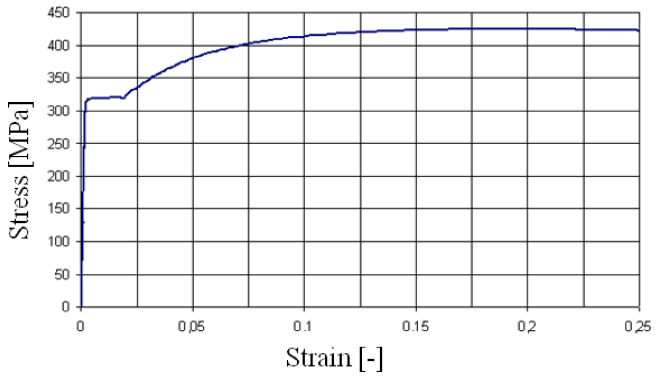

Fig. 7. The plot of the stress-strain relationship obtained from the tensile test for plate material S235JR2 (according to the European standard EN 10025:1990)

Based on the analysis of the test results, the following material parameters were adopted for the numerical model:

Young's modulus E = 215 GPa;
Yield strength Re = 320 MPa;
Tangent modulus H = 700 MPa;
Tensile strength Rm = 430 MPa.
Poisson ratio $\nu = 0.31$.

The test plate was welded to the frame, what provided avoiding of deformation of the plate on the edges. Besides strong bending, there also appeared the state of tension.

The frame of the base stand was made of steel profiles, the steel S235JR2 of a square shape with dimensions of 120 $\times$ 120 mm and wall thickness of 5 mm (Fig. 8). The profiles were adequately cut and welded at the corners.

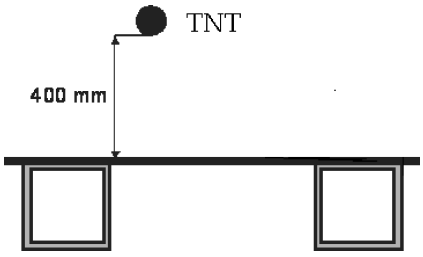

Fig. 8. The scheme of the test plate

The entire test plate had dimensions of 0.76 $\times$ 0.76 m. An open test zone had dimensions of 0.5 $\times$ 0.5 m (after excluding the test frame). The open test zone can be deformed freely.

The test-plates (Fig. 8) were loaded by a pressure wave (impulse) coming from detonations of an equivalent of 2 kg of TNT. The load was placed centrally above the plate at the distance of 0.4 m from the top surface of the plate.

3. The results of experimental studies

3.1. The experimental results for test 1. A general view of the test ground for test 1 is shown in Fig. 9. In the studies, an additional steel plate was used as a non-deformable base leveling a land effect on a permanent deformation of the test plate. Additional studies have shown superfluity of the abovementioned plate – there was no difference in the final deformation of the tested systems.

Fig. 9. The view of the experimental zone before putting in the detonator – Test 1

The test ground was loaded by a pressure wave coming from detonation of C4 explosive with a mass equivalent of 2 kg of TNT. The charge was placed at the distance of 0.4 m above the test plate.

As a result of the experiment, the permanent deformation of the test plate was obtained. A deformation size was initially measured using a straight edge and a caliper. A deformed base plate is illustrated in Fig. 10. Figure 10a presents a photograph of the test plate after the experimental study and 10.b shows a map of the permanent deformation obtained using a 3D scanner. As a result of measurements with a scanner, it was found that the permanent deformation of the plate was 0.3264 mm. This value was measured at the symmetry center of the plate, at the site of the largest deformation.

a)

b)

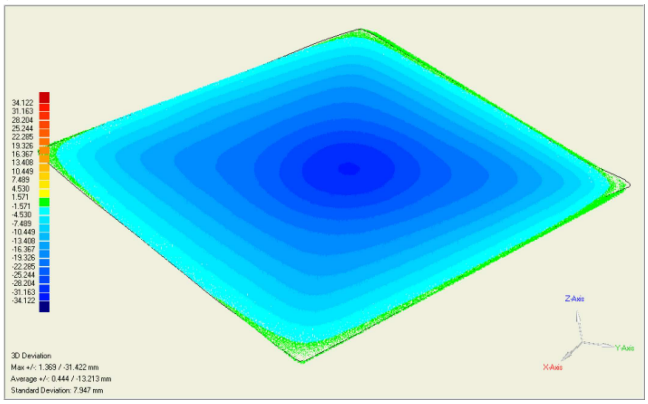

Fig. 10. Experimental zone after the experiment – Test 1: a) system after explosion, b) deformation map obtained by measuring with a 3D scanner

Due to problems with the symmetry of the load as well as the difficulty in adjusting the load (measurement errors), a deformation map of the test plate is asymmetrical. However, those differences are not glaring.

4. Numerical reaserch

4.1. Formulation of the physical model. The analysis of the impact of a pressure impulse on the structure was carried out with the use of a finite element method (FEM) with the explicit scheme of integration of equations of motion implemented in the MSC DYTRAN [11]. In those algorithms, the equilibrium equation of a discrete model (1.7) is solved by direct integration of time. These equations occur in a conjugate form, what results in a high numerical cost of their solutions and a high demand for memory in calculations.

The basic equation in an explicit approach, excluding damping due to short duration of the phenomenon, is as follows:

$$[M]\{\ddot{x}\}_n = \{F\}_n - \{F_{int}\}_n, \tag{7}$$

where $[M]$ – mass matrix, $\{F\}$ – matrix of external forces, $\{F_{int}\}$ – matrix of internal forces, n – step.

Assuming that the mass matrix occurs in a diagonal form, the equations of motion can be solved by the explicit Euler method. In this case, nodal acceleration vector $\{\ddot{x}\}$ can be determined from formula [8]:

$$\{\ddot{x}\}_n = [M]^{-1}(\{F\}_n - \{F_{int}\})_n. \tag{8}$$

In Eq. (8), damping can also be taken into account, however, also just as a diagonal matrix. An additional advantage of this approach is uncoupling of differential equations of motion, which enables their separate solution.

Velocity $\{\dot{x}\}_{n+1/2}$ and displacement $\{x\}_{n+1}$ vectors in subsequent time steps are obtained by integrating over time with the use of a central finite difference method [6]:

$$\begin{aligned} \{\dot{x}\}_{n+1/2} &= \{\dot{x}\}_{n-1/2} + \{x\}_n \Delta t_n, \\ \{x\}_{n+1} &= \{x\}_n + \{\dot{x}\}_{n+1/2} \Delta t_{n+1/2}. \end{aligned} \tag{9}$$

Unfortunately, this method is conditionally stable. In order to ensure the stability, the length of the integration step should be reduced:

$$\Delta T \leq 2/\omega_{\max}, \tag{10}$$

where $\omega_{\max}$ is first the highest frequency of free not-damped vibration of a discrete model. It means that the time step must be shorter than the time of the wave propagation through the smallest element in the calculation model. As a consequence, the more accurate the model (small elements) is, the integration step is shorter and computation time is longer. At the same time simultaneously the problem of the length selection vanishes.

Mechanical issues solved by computer modeling and simulations require adoption of an adequate description of behavior of the used materials. This description must take into account their specific characteristics, such as physical state, plasticity, brittleness, hardness.

4.2. Description of the numerical model. Numerical analysis was carried out for the structure which was loaded by a pressure wave generated by explosion of an explosive charge, which was placed centrally above the tested object (according to Table 1).

The pressure wave caused by detonation (approximately simulated detonation in point) was spreading in an area of a cube shape with assigned appropriate boundary conditions. The theoretical solution of propagation of strong discontinuity, with a spherical shape, initiated from a point source exists in the form of analytical equation of similarity formulated by Taylor. After transformation it can be written as (11):

$$p(r) = 0.155 E_0 r^{-3}, \tag{11}$$

where E_0 – initial internal energy, r – current radius of the sphere.

This allows for the computer simulation of a shock wave propagation process by assigning appropriate initial conditions (density, energy, pressure) to some selected elements of the Euler domain and solution laws of conservation of mass, momentum and energy. Typical values for the explosive substances are: density – 1600 kg/m^3, and specific internal energy – 4.2 MJ/kg. The space, in which the shock wave was spreading, was modelled using Euler type elements Hex 8 characterized by the ideal gas properties of $\gamma = 1.4$ and density corresponding to the density of atmospheric air at standard conditions ($\rho = 1.2829$ kg/m^3). An Euler cell size was selected on the basis of the numerical experiment described in author's previous works [21]. Since the calculations took into account the changes caused by deformation of the structure the structure was modelled using Lagrange elements of Shell Quad 4 type. Those elements have been given the following mechanical properties: $E = 2.15 \cdot 10^9$ MPa, $\nu = 0.31$. To describe behaviour of the steel, a bilinear model of elastoplastic material DYMAT 24 was used. The maximum strain failure criterion was adopted.

The development of a model of the structure was preceded by additional laboratory tests of mechanical properties of a steel armour. Laboratory research was carried out at the Department of Mechanics and Applied Computer Science, Military University of Technology.

A general view of the numerical model of the tested structure is shown in Fig. 11.

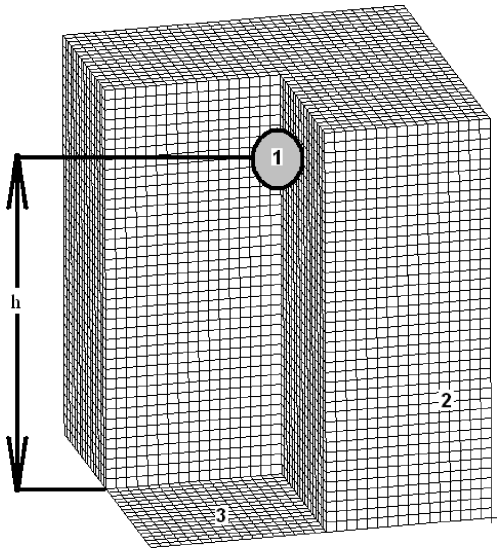

Fig. 11. Numerical model of the tested structure: 1 – an explosive, 2 – Eulerian domain, 3 – tested structure

4.3. The results of numerical analysis. The numerical model was loaded in the same way as in the experiment. According to the objective of publication, calculations were carried out for the explosive with the mass equivalent of 2 kg of TNT. The charge was placed at a distance of 0.4 m above the test plate for different angles of the plate arrangement. As a result of numerical analyses, there were obtained, among others, pressure maps and displacements charts, accelerations and speeds for characteristic points on the structure, especially for the center of the test plate. Additionally, there were studied the values of the strain energy and the hourglass energy (responsible for numerical errors).

The numerical analysis was based on the cube shaped, but suitably dense, The Euler element grid. The influence of the grid shape on the pressure on the forehead of the shock wave is relatively small [22]. The size of the Euler cell is important for reading pressure charts that gives pressure values for a particular Euler cell.

Numerical results for the test I.

Figure 12a shows distribution of the pressure acting on the test structure for the time $t = 4.484 \cdot 10^{-5}$ s.

Figure 12b illustrates distribution of the pressure acting on the test structure for the time $t = 1.043 \cdot 10^{-4}$ s, when a wave front reaches the tested structure.

Four areas of high pressure are located in the area where an explosive charge was placed. Those areas were the result of discretization of the model and do not affect the physics of phenomenon. One of the ways to avoid the occurrence of such phenomena is the proper formation of the Euler grid.

Figure 12c presents the amplification of the pressure impulse by reflection of the pressure wave from the barrier (for the time $1.6018 \cdot 10^{-4}$ s).

Figure 12d demonstrates the final deformation of the plate, there can be also observed a decrease of pressure in the Eulerian domain. In case of further analysis, the pressure in the Eulerian domain should be equalized to the initial atmospheric pressure.

Comparison of pressure values of the reflected wave for different angles of position of the plate is shown in Fig. 13.

The shortest time of arrival of the pressure for the tested cases were recorded, as predicted, for the plate placed at an angle of 45°.

Comparing the results of the numerical analysis, the most reliable are the charts. In the case of reading out the individual physical values from the plots, there is a possibility of a wrong approximation of the results.

The charts obtained for each test from the numerical analysis are very interesting. In the case of a permanent displacement, the largest displacement of the central node was noted for Test 4 while the smallest one for Test 1 (Fig. 14). These values are imposed by the distance between the load and the plane of the plate.

A comparison of the obtained results is shown in Table 2. In addition, this table presents the comparison between the results obtained in the experimental tests and the numerical analysis.

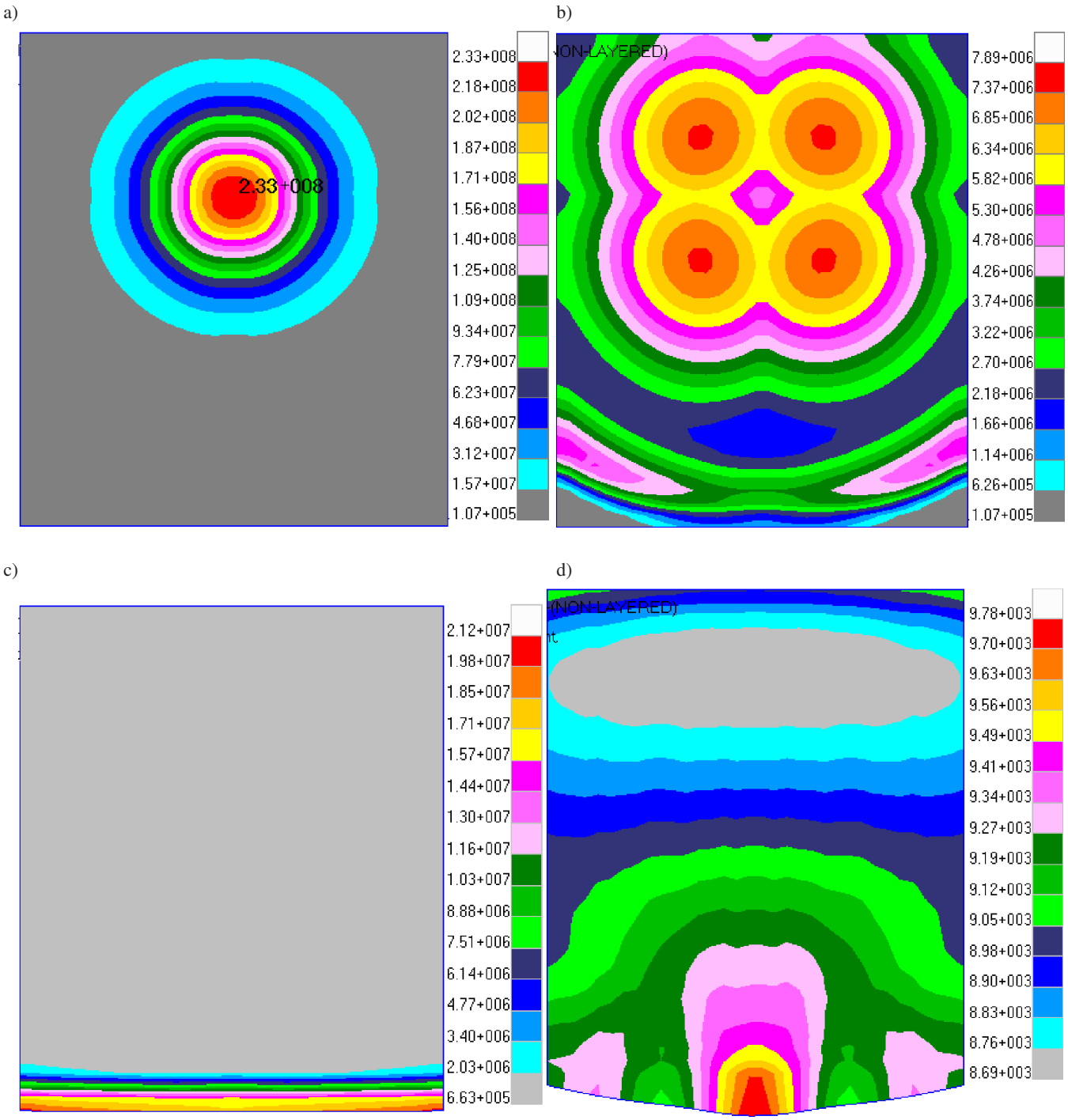

Fig. 12. Way of propagation of the pressure wave (interacting on the test plate) at different moments of time: a) $4.484 \cdot 10^{-5}$ s, b) $1.043 \cdot 10^{-4}$ s, c) $1.6018 \cdot 10^{-4}$ s, d) $2.0 \cdot 10^{-3}$ s

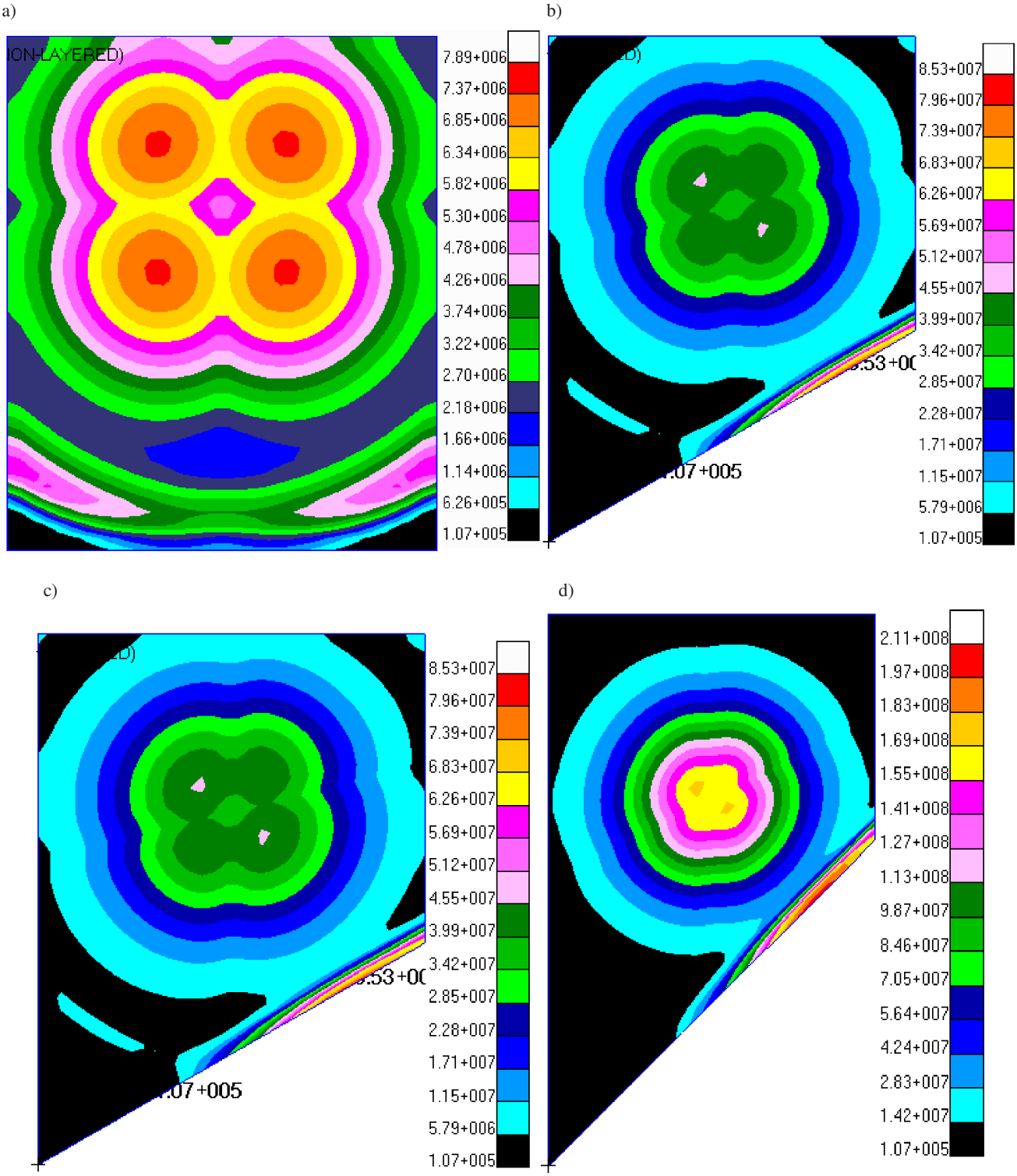

Fig. 13. Pressure maps, for the moment of reflection for different angles of position of the plate: a) 0° – 0.0001043 s, b) 15° – 6.9651 10^{-5} s, c) 30° – 6.9651 10^{-5} s, d) 45° – 5.3185 10^{-5} s

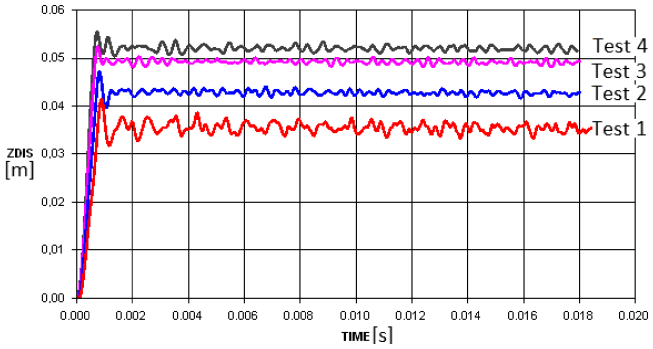

Fig. 14. Plots for central node displacement for individual tests

Table 2
Comparison of displacement for each test

Test	Numerical results – maximal displacement [m]	Numerical results – permanent displacement [m]
1	0.0413	0.0367
2	0.0469	0.0443
3	0.0523	0.0490
4	0.0560	0.0530

Figure 15 shows additionally the influence of the angle of the plate position on the permanent displacement of the central node. The interesting fact is that the largest displacement is observed for case 4 (an angle of 45°). It is worth noting that this value is rather illusory because it may seem to be that, from the mechanics of fluids, the greater the angle is, the most advantageous the flow around a plate should be. However, it is worth noting that the plate situated at the largest angle is the closest to the epicenter of the explosion. Therefore, taking into account formula 15, the pressure acting on the barrier is inversely proportional to the distance from the source of the explosion.

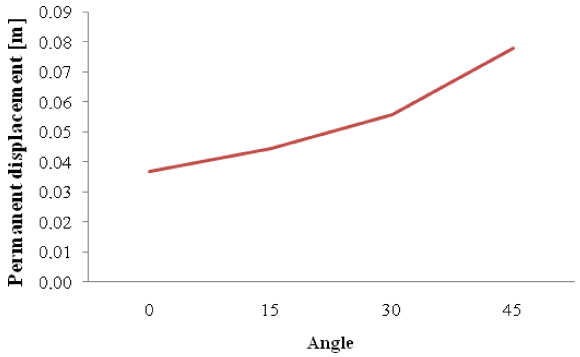

Fig. 15. Influence of changing the angle of the position of the test plate-on permanent displacement of the central node

The values of permanent displacements of the central node are similar to the results for accelerations, velocities and energies. The charts of the abovementioned values are shown in Figs. 16–18.

The maximum value of acceleration, as shown in Fig. 16, for a point in the plane of symmetry was approximately 10^6 m/s^2 for test 1. This value is so high (plainly not physical) as it is read out for a single node(located in the axis of symmetry).

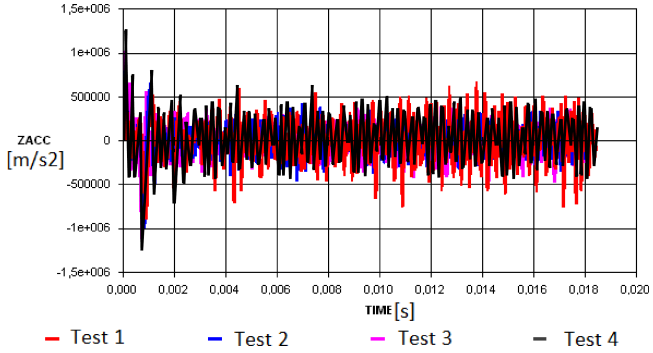

Fig. 16. The chart of acceleration for the node located on the upper wall of the object (in the plains of symmetry)

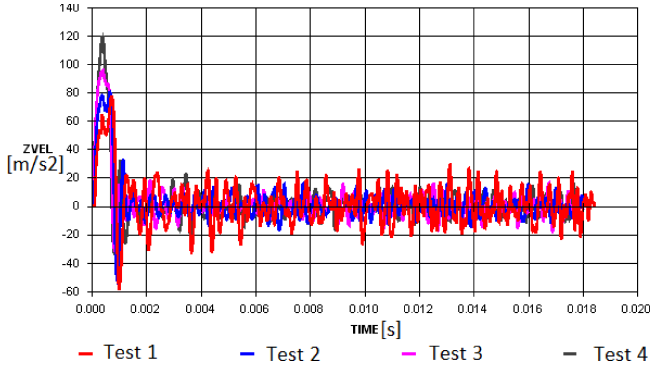

Fig. 17. Speed of the node located on the upper wall of the object (the plane of symmetry)

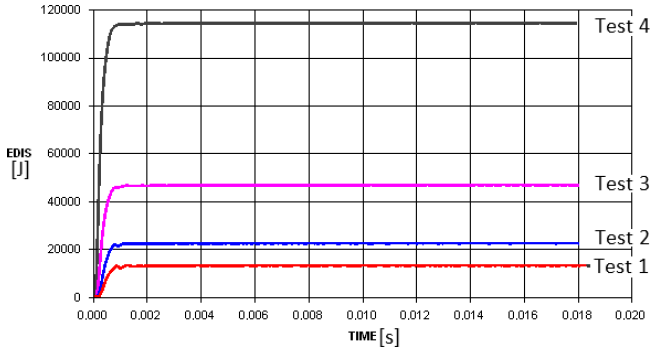

Fig. 18. Deformation energy for each test

Similarly as in the case of acceleration, the highest value of speed was recorded for test 4 – approximately 120 m/s (Fig. 17).

The highest value of the strain and the hourglass energy was read out for 4 test. The comparison of all extra physical quantities is shown in Table 3.

Table 3
Comparison of displacement for each test

Test	Speed [m/s]	Acceleration [m/s2]	Strain energy [J]	Hourglass energy [J]
1	77.069	944730	13068	0.70363
2	80.050	1005300	22430	2.61330
3	95.684	1021000	46793	10.79300
4	120.940	1244100	114510	15.84500

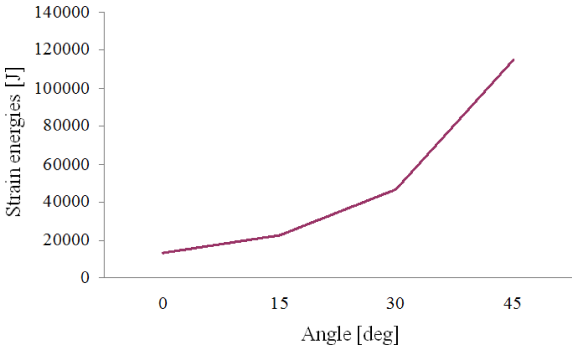

Fig. 19. Influence of changing the angle of the arrangement of the test plate on strain energies

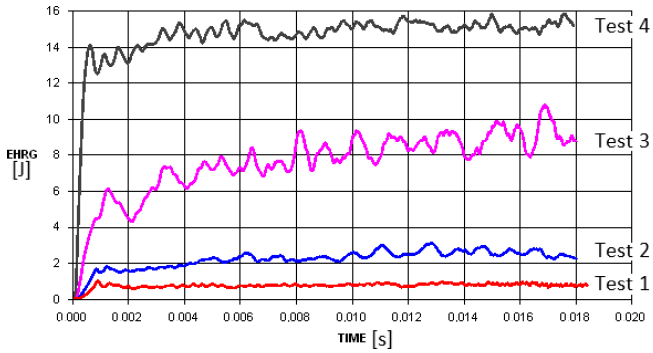

Fig. 20. Hourglass energy for each test

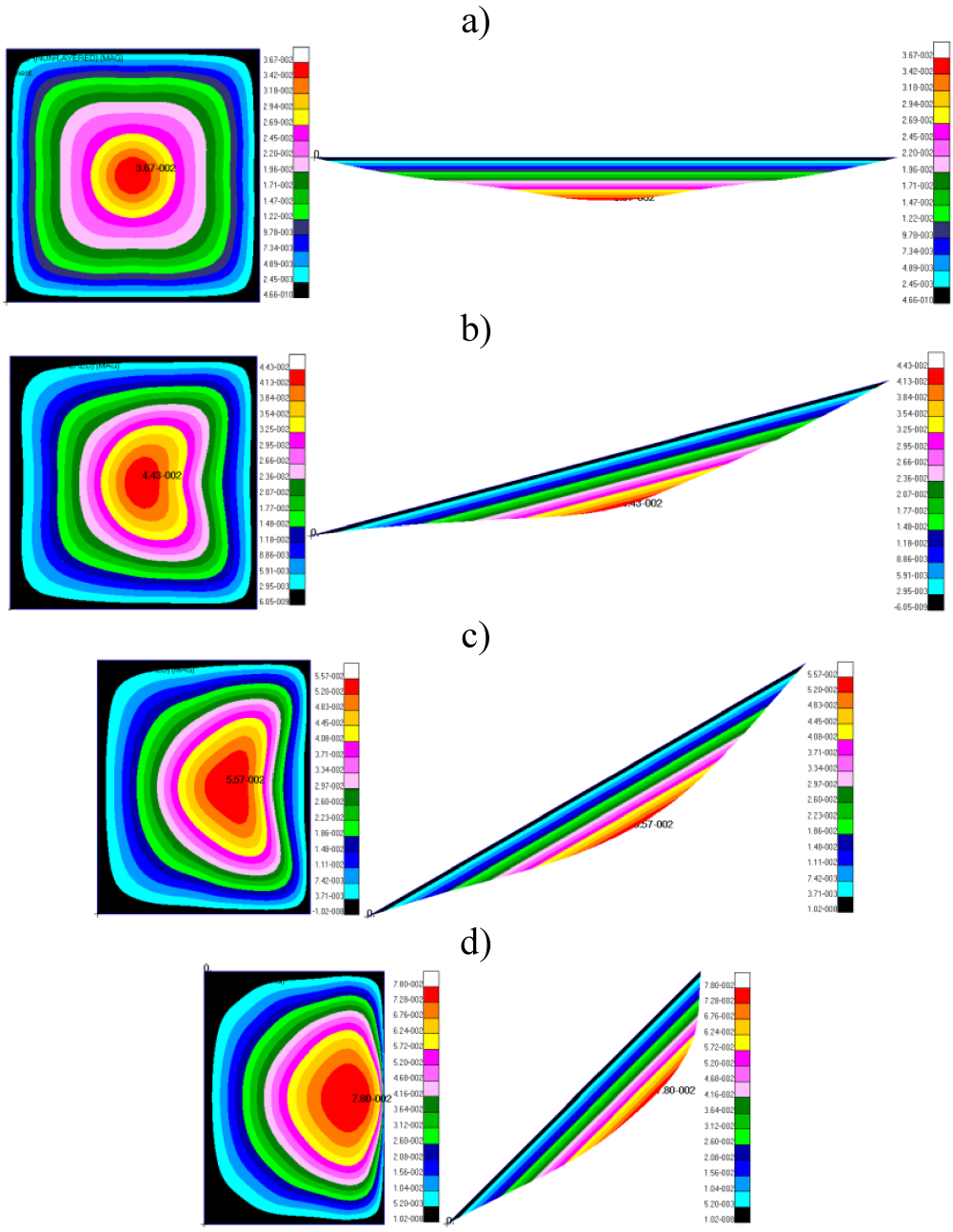

Fig. 21. Map of displacements: a) test 1, b) test 2, c) test 3, d) test 4

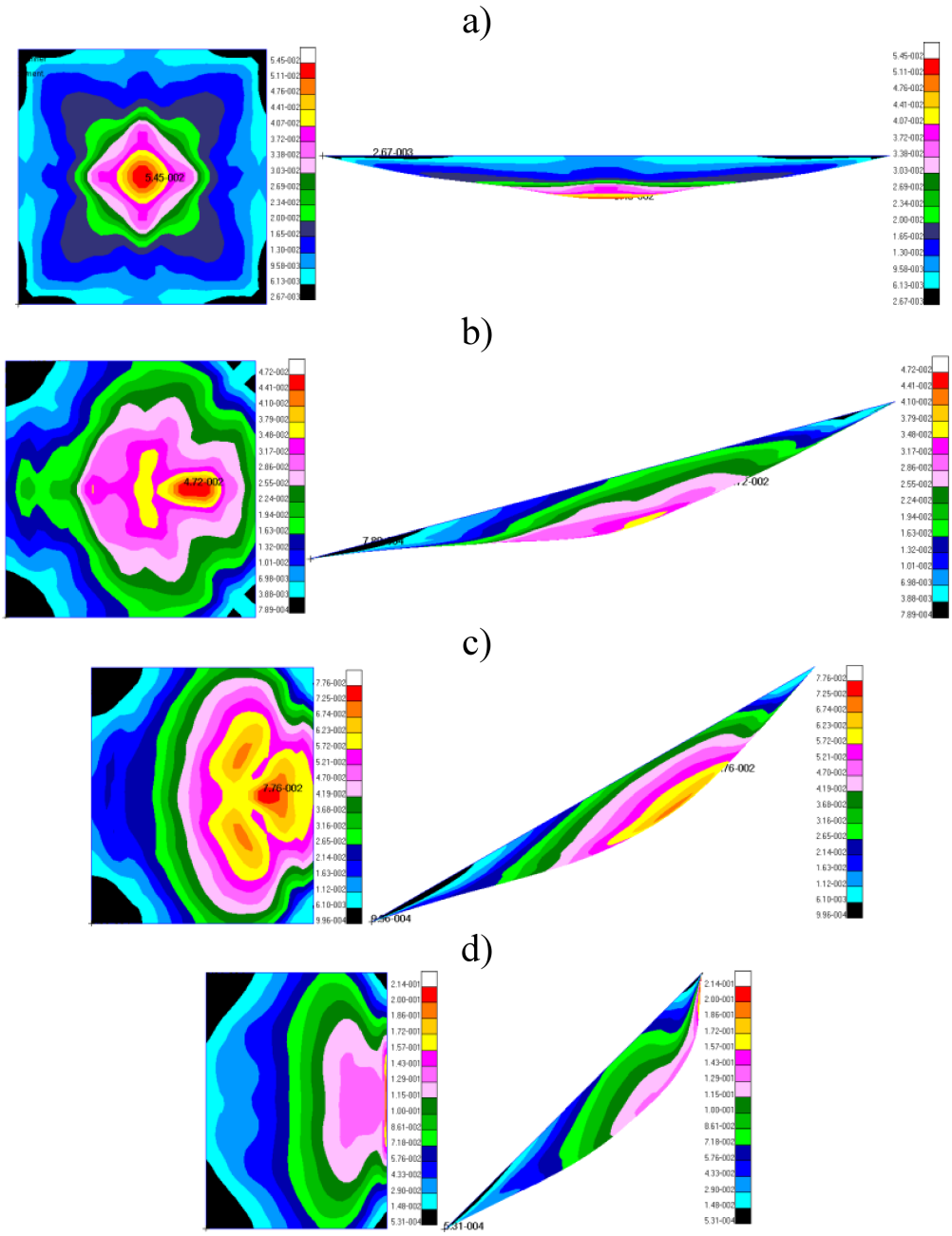

Fig. 22. Maps of plastic deformations a) test 1, b) test 2, c) test 3, d) test 4

Similarly as for a permanent displacement of the central node of the plates, strain energy values are comparable. The highest value of strain energy was recorded for test 4, Fig. 19.

Similarly as in the case of the graphs, additional physical quantities obtained from numerical analysis such as maps of: displacement, strain and equivalent tensile stress are shown in Figs. 21–23. All the maps were characterized by symmetry (which proves the correctness of modeling of the problem).

The values of permanent displacements were described previously. An interesting strain of the test plate is presented in Fig. 21. As in the case of displacements, the maximum values of the permanent deformation for each test are equal to: 3.67 10^{-2} m, 4.43 10^{-1} m, 5.57 10^{-1} m and 7.8 10^{-2} m, respectively (the highest for test 4).

The maximum values for permanent strains for each test are equal to: 5.45 10^{-2}, 4.72 10^{-2}, 7.76 10^{-2} and 2.14 10^{-1}, respectively (the highest are for Test 4). Maps of plastic deformations are shown in Fig. 22.

The maximum values for von Mises stresses for each test are equal to: 983 MPa, 592 MPa, 1060 MPa and 101 Mpa, respectively (the highest are for Tests 3 and 4). Von Mises stresses for the test plate are shown in Fig. 23. They point to the correct physical values previously obtained for the test plates. Such high values for von Mises stresses for steel are caused by the dynamic hardening of material and inertial effects, like hydrostatic compression of a medium.

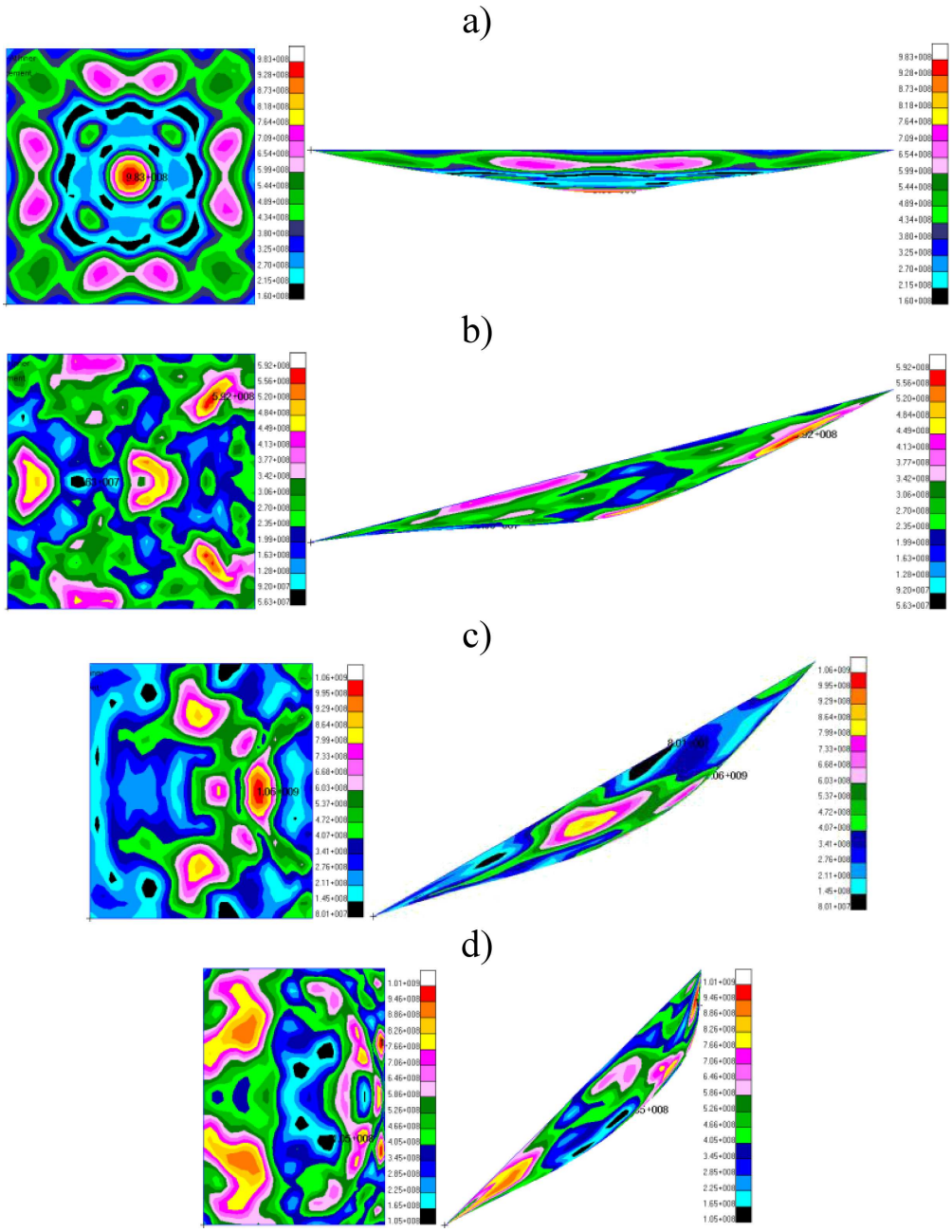

Fig. 23. Von Mises stress: a) test 1, b) test 2, c) test 3, d) test 4

5. Conclusions

The paper presents the results of the experimental studies and the numerical analysis of the influence of angle of the test plate position on its permanent deformation. In numerical analysis there was applied ALE coupling of Eulerian domain (describing the air) and Lagrangian domain (describing structures). In numerical analysis, the gas was characterized by air parameters. All kinds of material data have been selected on the basis of experimental studies and available literature. The plates were described using a piecewise linear plastic material model with dynamic strengthening.

During the tests of the test plate response for a various size of charges, an innovative test stand was used. The aim of the study was to validate numerical models taking into account the aspect of constitutive equations describing the material model and the selection of a model of explosion and a medium in which the pressure impulse spreads.

It is worth noting that one of the constants characterizing the system was the plate thickness and the distance of the charge of 2 kg of TNT from the bottom edge of the plate.

Examining an influence of an angle of the plate position on the dynamic responses of the system results in the possible use of these tests to evaluate, among others, the response of deflectors mounted on vehicles, exposed to explosion, at the side of the located charge.

The aforementioned case can be applied to determine an optimal angle of the deflector in the aspect of a side explosion in respect to a military vehicle.

Additionally, numerical studies can be used to validate numerical models in the context of the explosive and a constitutive model describing the barrier.

This issue is quite important from the point of view of the military vehicle's crew protection.

REFERENCES

[1] R. Krzewiński, *Explosion Dynamics. Part I. Methods of Loads Estimation,* WAT, Warsaw, 1982, (in Polish).

[2] К.П. Станюкович, Физикавзрыва Наука, Наука, Moscow, 1975.

[3] S.B. Menkes and H.J. Opat, "Tearing and shear failures in explosively loaded clamped beams", *Exp. Mech.* 13, 480–486 (1973).

[4] R.G. Teeling-Smith, and G.N. Nurick, "The deformation and tearing of thin circular plates subjected to impulsive loads", *Int. J. Impact Eng.* 11 (1), 77–91 (1991).

[5] G.N. Nurick and G.C. Shave, "The deformation and tearing of thin square plates subjected to impulsive loads-an experimental study", *Int. J. Impact Eng.* 18 (1), 99–116 (1996).

[6] K.W. Genson, "Vehicle shaping for mine blast damage reduction", *MSc Thesis,* University of Maryland, Maryland, 2006.

[7] R. Benedetti, "Mitigation of explosive blast effects on vehicle floorboard", *MSc Thesis*, University of Maryland, Maryland, 2008.

[8] S. Chung Kim Yuen, G.S. Langdon, G.N. Nurick, and E.G. Pickering, "Response of V-shape plates to localised blast load", *Proc. IMPLAST Conf.* 1, 1–11 (2010).

[9] O.C. Zienkiewicz and R.L. Taylor, *The Finite Element Method*, Butterworth-Heinemann, Oxford, 2000.

[10] M. Dacko, *The Finite Element Method in the Construction Mechanics*, Arkady, Warsaw, 1994, (in Polish).

[11] Dytran, *Theory Manual*, MSC, 2004.

[12] LS-DYNA *Theoretical Manual*, MSC, 1998.

[13] E. Włodarczyk, *Introduction to Explosion Mechanics*, PWN, Warsaw, 1994, (in Polish).

[14] W. Barnat, R. Gieleta, and T. Niezgoda, "Experimental investigation of selected explosion parameters for numerical model validation", *J. KONES Powertrain and Transport* 19 (4), 1–13 (2012).

[15] E. Krzystała, S. Kciuk, and A. Mężyk, *Identification of Threat to Special Vehicles' Crews During Explosion*, Silesian University of Technology, Gliwice, 2013, (in Polish).

[16] W. Barnat, "Experimental and numerical study of the impact of blast wale created by explosive charge on the steel plate", in *Review and Current Trends in Stability Structures. A Series of Monographs*, Lodz University of Technology, Łódź, 2013.

[17] W.E. Baker, *Explosions in Air*, University of Texas Press, London, 1973.

[18] P.D. Smith and J.G. Hetherington, *Blast and Ballistic Loading of Structures*, Butterworth-Heinemann, London, 1994.

[19] T. Stompor, *Structure and Exploitation of Ammunition. Striking Effects of Ammunition*, WAT, Warsaw, 1979, (in Polish).

[20] W. Barnat, *R00-O0037/3 Composite Panels To Vehicle Protection Against Effects of Temporary Explosive Charges*, WAT, Warsaw, 2010, (in Polish).

[21] W. Barnat and J. Kończak, *Introduction to Design Light Crawlers*, Military Year, Warsaw, 2011, (in Polish).

[22] W. Barnat, *Selected Problems of Energy Consuming New Types Protective Panels loaded by an Explosive Wave,* BellStudio, Warsaw, 2010, (in Polish).